Distribution of pore flow flux in binary granular packings

Hongli Shao¹, Kuang Cheng², Zhijie Zhang³, and Ha H. Bui⁴

¹College of Civil Engineering and Architecture, Hebei University, Baoding 071002, China; e-mail: shaohongli 2002@163.com.

²College of Civil Engineering and Architecture, Hebei University, Baoding 071002, China:

Department of Civil Engineering, Monash University, Australia; e-mail:

kcheng@hbu.edu.cn. Corresponding author.

³College of Civil Engineering and Architecture, Hebei University, Baoding 071002, China; e-mail: 15081438926@163.com.

⁴Department of Civil Engineering, Monash University, Australia; e-mail: ha.bui@monash.edu.

ABSTRACT

Binary granular packing is mainly characterized by mixture of finer and coarser particles which is often encountered in geotechnical engineering, e.g., gap-graded soils. The hydraulic and erosion properties of binary granular packings have gained special attention due to its close relation to the safety of earth structures, e.g., internal erosion of gap-graded soils in dam foundations. The pore flow distribution within the voids of the coarse skeleton is a key factor that affects the hydraulic properties and erosion process in binary granular packings, while a further understand on it is still needed. For this purpose, a semi-resolved CFD-DEM model was adopted to obtain the probability density distributions of pore flow flux within the voids of coarse skeleton in typical binary sphere packings. Delaunay triangulation was used to discretize the voids of coarse skeleton into individual pore element and, thereby, facilitate the calculation of pore flow flux through each pore throat. The results reveal that the distribution of pore flow flux changes obviously and becomes more uniform with the transition of the binary packing from underfilled to overfilled packings. However, the size ratio between coarser and finer particles has a negligible influence on the transition in the distribution.

Keywords: Internal erosion; Suffusion; Pore flux rate

INTRODUCTION

Binary granular packing is mainly characterized by mixture of finer and coarser particles with the absence of medium-sized particles. It is often encountered in geotechnical engineering, e.g., gap-graded soils. The finer particles may be eroded from the binary

granular packing under seepage flow, which is referred to as suffusion, a typical mode of internal erosion. The erosion of finer particles may weaken the strength of the granular packing and, thereby, have great threats to earth structures such as embankment dams (Luo et al. 2017; Johnston et al. 2023) and colluvium slopes (Cui et al. 2017). The fundamental mechanism of suffusion involves the interaction between the fine particle loss and the development of preferential flow. The pore flow distribution within the voids of the coarse skeleton is a key factor that affects the suffusion process.

Several research (Datta et al. 2013; Nguyen and Papavassiliou. 2021; Bijeljic et al. 2013; Alim et al. 2017) have focused on the distribution of pore fluid flow within granular packings. Datta et al. (2013) obtained the distribution of fluid velocity within the pores of 3D sphere packings using transparent medium and confocal microscopy. Note that the pores of the granular packings were divided into interrogation windows with dimensions of around 1/10 of particle diameter to obtain the pore fluid velocity using Particle Image Velocimetry (PIV). The probability density function (PDF) of pore fluid velocity was found to approximately have an exponential decay. Nguyen and Papavassiliou. (2021) proposed a more general distribution, i.e., Weibull distribution, for the pore fluid velocity in various porous media. They demonstrated that the pore size distribution appeared to be important for the form of the velocity distribution. Alim et al. (2017) focused on the flow rate through each pore throat. They found that the PDF of pore flow rate also follows an exponential distribution for random granular packing. Meanwhile, Alim et al. (2017) demonstrated that the local correlation of pore sizes, instead of the overall pore size distribution, set the exponential PDF of pore flow rate.

Only granular particles with very narrow and simple PSDs were considered in previous research (Zarrei et al. 2022; Datta et al. 2013; Sanvitale et al. 2023). Binary granular packings often have very broad PSDs with large size differences between coarser and finer particles. The distributions of pore fluid flow within binary granular packings may be more complex compared to those observed within granular media with very narrow and simple PSDs. However, there is still a lack of study on pore flow distribution in binary granular packings.

This study focuses on the pore flow distribution in binary sphere packings. The distributions of pore flux rate within voids of coarse skeleton in binary sphere packings were investigated using the semi-resolved coupled Computational Fluid Dynamics (CFD) - Discrete Element Method (DEM) previously developed by the authors (Cheng et al., 2018). The capability of the semi-resolved CFD-DEM method in reproducing the pore flow distribution in granular packings was thoroughly examined by comparing to experimental results. Then, the influence of content of finer particles and size ratio between coarser and finer particles on the distribution of pore flow rate was studied.

SEMI-RESOLVED CFD-DEM METHOD

The coupled CFD - DEM is a promising tool for modeling the interactions between fluid and granular particles (Tsuji et al. 1993). In this method, the CFD is used to model the

fluid flow while the DEM is adopted to simulate the particle motion. The fluid flow-particle interactions can be treated in different ways based on different resolved scales of fluid flow (Tsuji et al. 1993; Sharma and Patankar 2005; Cheng et al. 2018). The semi-resolved CFD-DEM method is designed for modeling fluid-particle interactions in binary granular packings, especially for situations involving finer particle migration under seepage flow (Cheng et al. 2018). In the semi-resolved method, the pore fluid flow within the voids of coarse skeleton formed of coarser particles is resolved using the fictitious domain method (Glowinski et al. 1999; Sharma and Patankar 2005), while the finer particle-fluid interactions are treated by locally averaging (Anderson and Jackson 1967). By doing so, the detailed pore fluid flow within the voids of coarse skeleton is obtained, and meanwhile the computational burden is reduced by using a simplified way, i.e., a locally averaging, for the coupling between the finer particles and pore fluid flow. For more details of the semi-resolved CFD-DEM method, please refer to Cheng et al. (2018).

NUMERICAL MODLE

Binary sphere packings

Different binary sphere packings consisting of coarser and finer particles were considered. Their particle size distributions (PSDs) are illustrated in Figure 1.

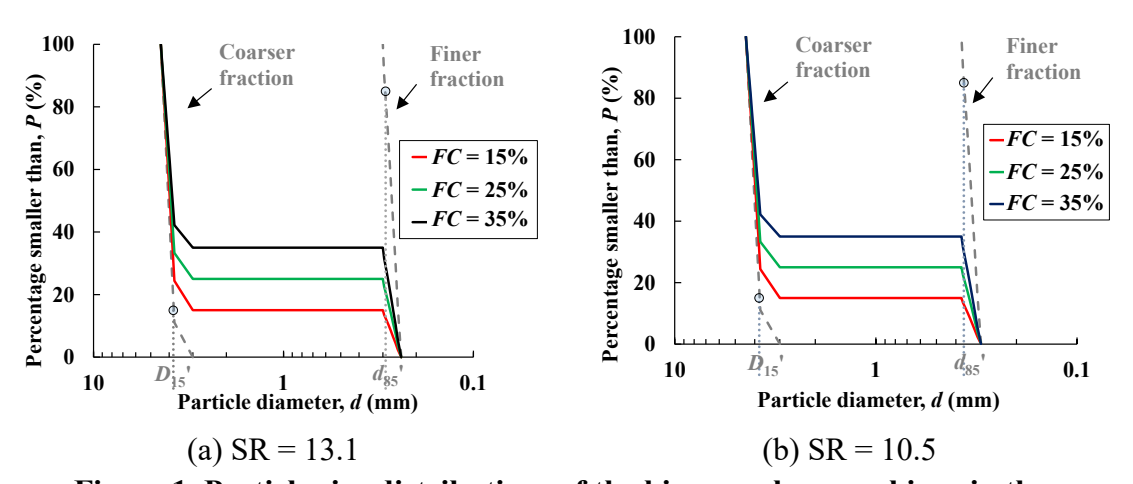


Figure 1. Particle size distributions of the binary sphere packings in the numerical simulations (FC represents content of finer particles; $SR = D_{15}'/d_{85}'$ is the size ratio between coarser and finer particles)

Two different size ratios between coarser and finer particles, i.e., SR = 10.5 and 13.1, and three different contents of finer particles, i.e., fine content FC = 15%, 25% and 35% are considered. Additionally, sphere packings composed of only coarse particles

were also considered for comparison.

Model setup

The semi-resolved solver (Cheng et al. 2018) implemented based on CFDEM program (Goniva et al. 2010) was used in the current simulations. As shown in Figure .2, rectangle samples were modeled with a height of 28 mm and a side length of 18.75 mm. Periodic boundary conditions were used for lateral boundaries both in the DEM and CFD sides to reduce boundary effect. Radius expansion approach (O'Sullivan 2011) was adopted for the generation of samples to target porosities.

In the DEM side, Hertz-Mindlin model incorporated with a rolling resistance model was used for resolved the particle contact; see Cheng et al. (2017) for more details on this contact model. The particle properties required by the contact model were summarized in Table 1; these parameters were calibrated for quartz sand particles in our previous study (Cheng et al. 2017). The DEM timestep was set to 2×10^{-7} s, which is around one-seventh of the critical Rayleigh time to guarantee the numerical stability (Cheng et al. 2024). Gravity was not considered to avoid the segregation of finer and coarser particles. On the other hand, the finer particles should be easily transported by seepage flow due to the absence of gravity, which will further result in inhomogeneous samples. For simplicity, the particles were fixed artificially to keep the samples relatively homogeneous in the simulations.

Table 1. Material properties and computational settings.

Particle properties			
Density, ρ _p (kg·m ⁻³)	2650	Rolling stiffness coefficient, $\alpha_{\rm r}$ 0.193	
Young's modulus, E_p (GPa)	1×10 ⁹	Restitution coefficient, e	0.9
Poisson's ratio, v_p	0.2	Coarse particle diameters, (mm)	3.75-4.425
Sliding friction coefficient, μ_s	0.84	Fine particle diameters, (mm)	0.24-0.3
Rolling friction coefficient, $\mu_{\rm r}$	0.26		0.3-0.375
Fluid properties			
Density, $\rho_f(\text{kg}\cdot\text{m}^{-3})$	1000	Dynamic viscosity, μ_f (kg·m ⁻¹ ·s ⁻¹)	1×10^{-3}
Computational settings			
DEM time step, $\Delta t_{\rm DEM}$ (s)	2×10^{-7}	CFD time step, Δt_{CFD} (s)	2 .5× 10 ⁻⁴
Bandwidth of Gaussian function, $b_{\rm w}$ (mm)	2	Coupling interval, N_c 1250	

In the CFD side, periodic boundary conditions were imposed on four lateral boundaries, while pressure boundary conditions were applied on the top and bottom of the fluid domain. The hydraulic gradient, $i=(p_i-p_o)/\rho_f gH_s$, was increased step-wised as shown in Figure 3, where p_i and p_o are the pressure at the inlet and outlet, respectively, H_s is the sample height, ρ_f is the fluid density, g is the gravitational acceleration. Hexahedral fluid meshes were used to discretize the fluid domain, as shown in Figure .2

It is noteworthy that the fluid meshes are overlapped with coarser particles, which is an advantage of the fictitious domain method used in the semi-resolved CFD-DEM model. Different mesh sizes were considered for sensitive analysis of fluid mesh, which will be detailed in Section 4. The fluid properties were set to be those of pure water under standard conditions (20°C, 1 atm), with the specific parameters detailed in Table 1. The CFD timestep is set to be $\Delta t_{\text{CFD}} = 2.5 \times 10^{-4} \text{ s}$.

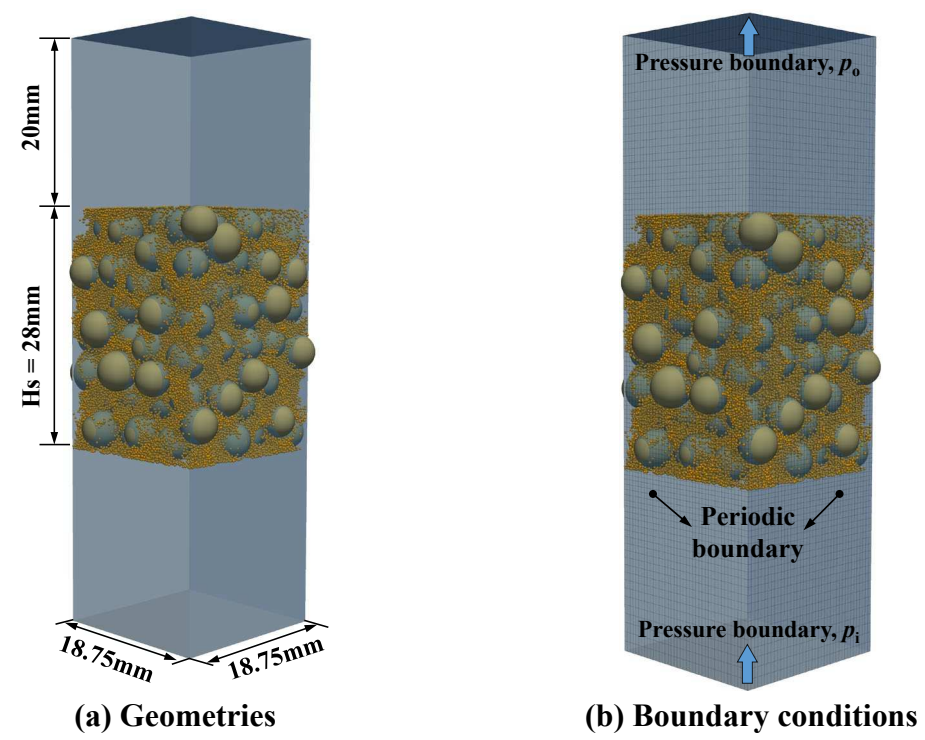


Figure 2. Geometries and boundary conditions of the numerical model.

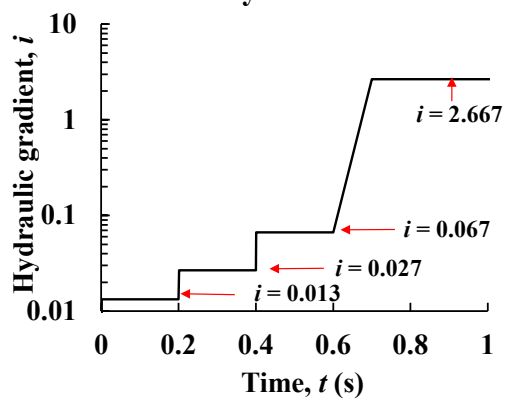


Figure 3. Hydraulic gradient used in the simulations

The coupling of DEM and CFD requires the translation between the Eulerian fields (e.g., porosity, velocity, pressure in fluid meshes) and Lagrangian fields (e.g., particle velocity carried by each particle). A mesh-independent approach, i.e., Gaussian-

based approach developed in our previous research (Yang et al. 2019) was used for the Eulerian-Lagrangian fields translation. In this approach, the bandwidth $b_{\rm w}$ was needed and set to be two times of the maximum diameter of finer particles as suggested by our previous study (Yang et al. 2019). Table 2 summarizes the details of the binary sphere packings samples used in the simulations.

Table 2. The binary sphere packings samples used in the simulations.

Sample number	Content of finer particles, FC (%)	Void ratio, e	Number of particles
FC-0 ^a	0	0.845	147
FC15-Gap13.1 b	15	0.554	87950
FC15-Gap10.5 °		0.555	45103
FC25-Gap13.1	25	0.403	146466
FC25-Gap10.5	25	0.442	75055
FC35-Gap13.1	35	0.315	204975
FC35-Gap10.5		0.333	105003

^a FC-0 represents that the binary sphere packings sample contains only coarser particles.

MODEL VALIDATION

Fundamental validations have been conducted on the semi-resolved CFD-DEM method in treating particle-fluid interactions in our previous research (Cheng et al. 2018; Yang et al. 2019). In the current study, we further examine the capability of the semi-resolved method in resolving the pore fluid flow in granular packings. For this purpose, probability density distribution of pore fluid velocity in granular packings were obtained and compared to the experimental results. To the authors' knowledge, the pore fluid flow in binary granular packings is difficult to be obtained in the experiments due to the relatively large difference between the coarser and finer particles. Therefore, only sphere packings with simple gradations were modeled for validation. For this purpose, sphere packing formed of only the coarser part (with diameters of 3.75 - 4.43 mm) of the binary spheres shown in Figure .2 were modeled using the semi-resolved method. The packing porosity is around 0.458. The particle Rynolds number is around 1×10^{-2} . The simulation results were then compared to the distribution of pore fluid velocity obtained in the experiments of Datta et al. (2013), in which sphere packings formed of uniformly-sized glass beads were tested. As shown in Figure .4, the probability density distributions of pore fluid velocity were obtained in the numerical simulations with different mesh sizes,

^b Gap13.1 represents size ratio is 13.1.

^c Gap10.5 represents size ratio is 10.5.

i.e., $L_{\rm m} = \frac{d}{3.8}$, $\frac{d}{6}$, $\frac{d}{9.6}$, and $\frac{d}{15}$, where d is the particle diameter. Note that the velocity magnitude $u_{\rm mag}$ was normalized by the averaged interstitial velocity $u_{\rm D}/n$.

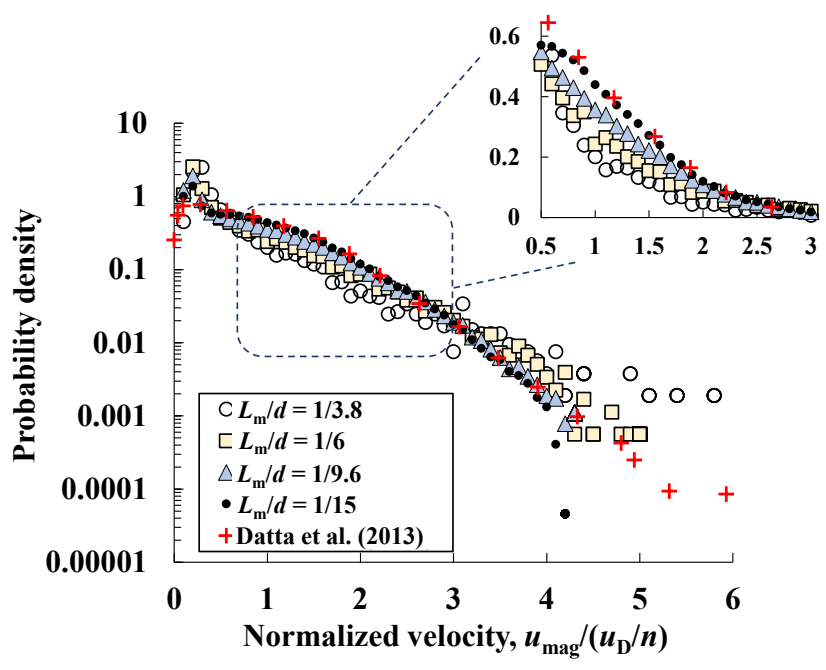


Figure 4. Probability density distribution of normalized fluid velocity $u_{\text{mag}}/(u_{\text{D}}/n)$: Numerical results obtained at different mesh resolutions and comparison to experimental observations in Datta et al. (2013)

It can be seen that the velocity distribution tends to be converged with the refinement of fluid mesh. It changes little as $L_{\rm m}$ is smaller than $\frac{d}{9.6}$. Therefore, $L_{\rm m}=\frac{d}{9.6}$ was used in the following simulations. For simulations with $L_{\rm m} \leq \frac{d}{9.6}$, the probability density distributions present an exponential decay, which is very similar to that obtained in the experiment. Meanwhile, there is an abnormal peak near zero velocity which should be due to a lack of mesh resolution near the particle surface. Nevertheless, this discrepancy is considered to be acceptable for $L_{\rm m}=\frac{d}{9.6}$ since the most concerned in the current study is the averaged flow on each pore throat, instead of the detailed flow in each fluid mesh.

DISTRIBUTION OF PORE FLUX RATE

This study mainly focused on the averaged fluid flow on pore throats of the coarse skeleton. To this end, Delaunay triangulation was used to discretize the coarse skeleton into tetrahedrons and, meanwhile, discretize the pores of coarse skeleton into pore elements, as illustrated in Figure 5; note that the void of each tetrahedron represent a pore element, while the space outside coarse particles on each surface of the tetrahedron denotes the pore throat.

Pore flux rate, U_0 [m/s], was defined on each surface of the tetrahedron as the volume of fluid passing through unit area of pore throat in unit time as follow.

$$U_{\rm o} = \frac{Q_{\rm o}}{A_{\rm o}}$$
,

in which, Q_0 [m³/s] is the flow rate defined as the volume of fluid passing through the pore throat in unit time; A_0 [m²] is the area of the pore throat.

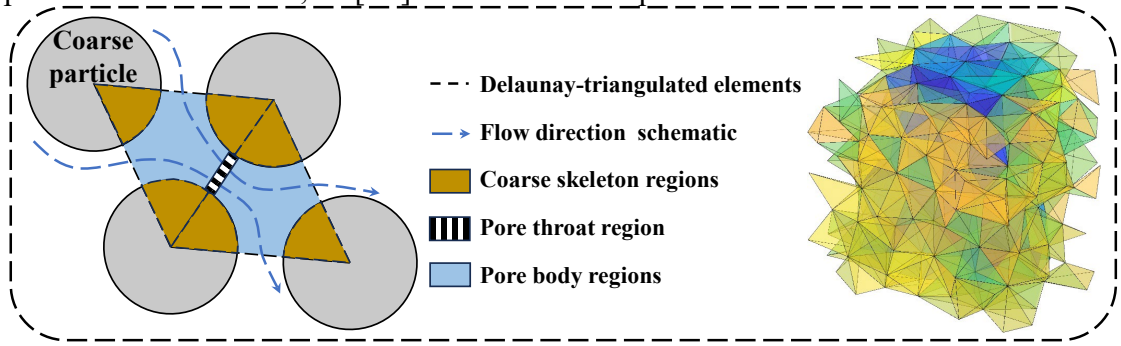


Figure 5. Schematics for pore element and pore throat discretized using Delaunay triangulation.

The probability density distributions of pore flux rate in the voids of coarse skeleton were obtained for binary granular packings with various contents of finer particles, FC, and different size ratios, SR, as shown in Figure 6 It is noteworthy that the pore flux rate U_0 was normalized by the mean value of pore flux rate $mean(U_0)$ within the granular packing. It can be seen that the distributions of pore flux rate remain around constant for the normalized pore flux rate smaller than one, while they decay exponentially for normalized pore flux rate larger than one. The size ratio has little effect of the distribution. On the other hand, the exponential decay becomes pronounced and the distribution is obviously narrowed as the content of finer particles, FC, exceeds around 25%. It indicates that the pore flow flux within the voids of coarse skeleton becomes more uniform with the increase of FC. Shire et al. (2014) demonstrated that the packing fabric of binary packing gradually transits from underfilled to overfilled packings as the content of finer particles exceed 24% - 35%. That is to say, the distribution of pore flow flux within the voids of coarse skeleton changes obviously and tends to be uniform as the binary packing transits from underfilled to overfilled packings. It indicates that the pore structure of coarse skeleton has an obvious change and tends to be uniform with the transition from underfilled to overfilled packings in binary packings.

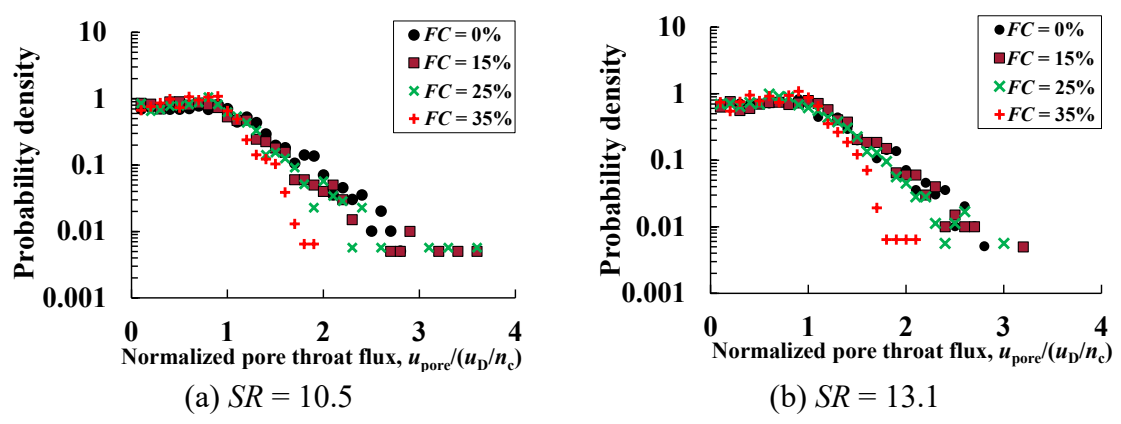


Figure 6. Probability density distributions of pore flux rate for binary granular packings with various contents of finer particles, FC, and different size ratios, SR (the pore flux rate U_0 was normalized by the mean value of pore flux rate $mean(U_0)$ within the granular packing)

CONCLUSIONS

This study investigated the pore flow distribution in binary granular packings. For this purpose, a semi-resolved CFD-DEM model was adopted to obtain the probability density distributions of pore flow flux within the voids of coarse skeleton in typical binary sphere packings. The effects of content of finer particles and size ratio between coarser and finer particles were examined. Delaunay triangulation was used to discretize the voids of coarse skeleton into individual pore element and, thereby, facilitate the calculation of pore flow flux through each pore throat.

The results reveal that the distribution of pore flow flux within the voids of coarse skeleton changes obviously and becomes more uniform with the transition of the binary packing from underfilled to overfilled packings (i.e., as the content of finer particles increases from 25% to 35%). It indicates a clear evolution in the pore structure of the coarse skeleton, which becomes more homogeneous with the transition from underfilled to overfilled packings. However, the particle size ratio has a negligible influence on the transition in the distribution.

ACKNOWLEDGEMENTS

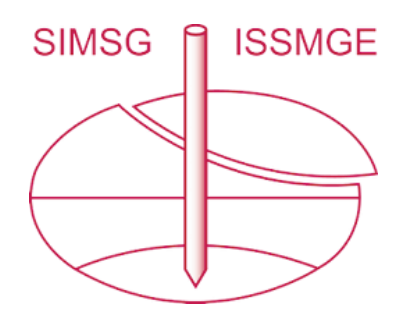
This study was supported by the National Natural Science Foundation of China [grant number 52009025]. The author, Kuang Cheng, gratefully acknowledges the support of the China Scholarship Council (CSC) for his postdoctoral research at Monash University. The computing and technical supports from the High-Performance Computing Center of Hebei University and the National Computational Infrastructure (NCI Australia) are acknowledged. The authors would like to thank Tien Nguyen (MCG Lab, Monash University) for his technical support in compiling and running the software on the

REFERENCES

- Alim, K., Parsa, S., Weitz, D. A., and Brenner, M. P. (2017). "Local pore size correlations determine flow distributions in porous media." *Phys. Rev. Lett.*, 119, 144501.
- Anderson, T. B., and Jackson, R. O. Y. (1967). "Fluid mechanical description of fluidized beds. Equations of motion." Ind. Eng. Chem. Fundam., 6(4), 527-539.
- Bijeljic, B., Raeini, A., Mostaghimi, P., and Blunt, M. J. (2013). "Predictions of non-Fickian solute transport in different classes of porous media using direct simulation on pore-scale images." *Phys. Rev. E*, 87(1), 013011.
- Cheng, K., Wang, Y., Yang, Q., Mo, Y. B., and Guo, Y. (2017). "Determination of microscopic parameters of quartz sand through tri-axial test using the discrete element method." *Comput. Geotech.*, 92, 22-40.
- Cheng, K., Wang, Y., and Yang, Q. (2018). "A semi-resolved CFD-DEM model for seepage-induced fine particle migration in gap-graded soils." *Comput. Geotech.*, 100, 30-51.
- Cheng, K., Ping, X., Han, B., Wu, H., and Liu, H. (2024). "Study on particle loss-induced deformation of gap-graded soils: Role of particle stress." *Acta Geotech.*, 19(12), 7865-7892.
- Cui, Y. F., Zhou, X. J., and Guo, C. X. (2017). "Experimental study on the moving characteristics of fine grains in wide grading unconsolidated soil under heavy rainfall." *J. Mt. Sci.*, 14(3), 417-431.
- Datta, S. S., Chiang, H., Ramakrishnan, T. S., and Weitz, D. A. (2013). "Spatial fluctuations of fluid velocities in flow through a three-dimensional porous medium." *Phys. Rev. Lett.*, 111(6), 064501.
- Glowinski, R., Pan, T. W., Hesla, T. I., Joseph, D. D., and Périaux, J. (1999). "A distributed Lagrange multiplier/fictitious domain method for particulate flows." *Int. J. Multiph. Flow*, 25(5), 755-794.
- Goniva, C., Kloss, C., Hager, A., and Pirker, S. (2010). "An open source CFD-DEM perspective." Proc., OpenFOAM Workshop, Göteborg, 22-24.
- Johnston, I., Murphy, W., and Holden, J. (2023). "Alteration of soil structure following seepage-induced internal erosion in model infrastructure embankments." *Transp. Geotech.*, 42, 101111.
- Luo, Y., Nie, M., and Xiao, M. (2017). "Flume-scale experiments on suffusion at bottom of cutoff wall in sandy gravel alluvium." *Can. Geotech. J.*, 54(12), 1716-1727.
- Nguyen, V. T., and Papavassiliou, D. V. (2021). "Velocity magnitude distribution for flow in porous media." *Ind. Eng. Chem. Res.*, 60(38), 13979-13990.
- O'Sullivan, C. (2011). "Particle-based discrete element modeling: Geomechanics perspective." *Int. J. Geomech.*, 11(6), 449-464.
- Sanvitale, N., Zhao, B. D., Bowman, E. T., and O'Sullivan, C. (2023). "Particle-scale observation of seepage flow in granular soils using PIV and CFD." *Géotechnique*,

- 73(1), 71-88.
- Sharma, N., and Patankar, N. A. (2005). "A fast computation technique for the direct numerical simulation of rigid particulate flows." *J. Comput. Phys.*, 205(2), 439-457.
- Shire, T., O'Sullivan, C., Hanley, K. J., and Fannin, R. J. (2014). "Fabric and effective stress distribution in internally unstable soils." *J. Geotech. Geoenviron. Eng.*, 140(12), 04014072.
- Tsuji, Y., Kawaguchi, T., and Tanaka, T. (1993). "Discrete particle simulation of two-dimensional fluidized bed." *Powder Technol.*, 77(1), 79-87.
- Yang, Q., Cheng, K., Wang, Y., and Ahmad, M. (2019). "Improvement of semi-resolved CFD-DEM model for seepage-induced fine-particle migration: Eliminate limitation on mesh refinement." *Comput. Geotech.*, 110, 1-18.
- Zareei, A., Pan, D., and Amir, A. (2022). "Temporal evolution of erosion in pore networks: From homogenization to instability." *Phys. Rev. Lett.*, 128(23), 234501.

INTERNATIONAL SOCIETY FOR SOIL MECHANICS AND GEOTECHNICAL ENGINEERING



This paper was downloaded from the Online Library of the International Society for Soil Mechanics and Geotechnical Engineering (ISSMGE). The library is available here:

https://www.issmge.org/publications/online-library

This is an open-access database that archives thousands of papers published under the Auspices of the ISSMGE and maintained by the Innovation and Development Committee of ISSMGE.

The paper was published in the proceedings of the 12th International Conference on Scour and Erosion and was edited by Shinji Sassa as the Chair of the TC213 on Scour and Erosion. The conference was held in Chongqing, China from November 4th to November 7st 2025.